J Therm Anal Calorim (2012) 110:227–233
DOI 10.1007/s10973-012-2230-9

The influence of synthesis method and Mg–Al–Fe content on the thermal stability of layered double hydroxides

Tatjana Vulic · Andreas Reitzmann · Jonjaua Ranogajec · Radmila Marinkovic-Neducin

CEEC-TAC1 Conference Special Issue

Abstract Layered double hydroxides (LDHs) and their thermally derived mixed oxides have reached growing attention in past decades due to their wide application as catalysts or catalyst supports in organic/pharmaceutical synthesis, clean energy and environmental pollution control (decomposition of volatile organic compounds, photodecomposition, $DeNo_x$ and $DeSO_x$). Desired properties of LDHs can easily be tailored using different synthesis methods and introducing different bivalent and trivalent constituting metals. In this study, Mg–Al and Mg–Al–Fe LDHs were synthesized by low supersaturation (LS) and high supersaturation (HS) coprecipitation methods. The content of trivalent ions was varied in a wide range between $0.15 < x < 0.7$ exceeding the optimal range for the single LDH phase synthesis ($0.20 < x < 0.33$). The intention was to induce the formation of different LDHs and consequently obtain, after thermal treatment, different multiphase mixed oxides. The properties of the precipitates were investigated by structural (XRD), chemical (AAS and EDS) and thermal analysis (TG–DTA). The study revealed that the LS method allows the formation of LDHs with an extended M(III) substitution ($x = 0.5$). Although, a more disordered structure in the stacking of layers was detected for HS samples, LS samples with the same initial composition showed lower thermal stability estimated by lower temperature of both LDH thermal decomposition transition stages. The thermal stability of LDHs was not influenced considerably with the introduction of a small amount of iron as ternary metal even though lower crystallinity of Mg–Al–Fe LDHs was observed.

Keywords Anionic clays · Thermal decomposition · TG · DTA · Elemental chemical analysis

T. Vulic (✉) · J. Ranogajec · R. Marinkovic-Neducin
Faculty of Technology, University of Novi Sad, Bul. Cara Lazara 1, 21000 Novi Sad, Serbia
e-mail: tvulic@uns.ac.rs

A. Reitzmann
Institute of Chemical Process Engineering, Karlsruhe Institute of Technology (KIT), Fritz-Haber-Weg 2, 76131 Karlsruhe, Germany

Present Address:
A. Reitzmann
Süd-Chemie AG, Bruckmühl, 83052 Munich, Germany

Introduction

Layered double hydroxides (LDHs) and their thermally derived mixed oxides are being extensively investigated due their wide application as catalysts or catalyst supports in organic/pharmaceutical synthesis, clean energy (production of hydrogen and carbon nanotubes) and environmental pollution control (decomposition of volatile organic compounds, photodecomposition, $DeNo_x$ and $DeSO_x$) [1–5]. Also, the ability to tailor LDH properties using different synthesis methods and introducing different bivalent and trivalent constituting metals makes these materials interesting for scientific research [6]. LDHs, also known as hydrotalcite-like materials, belong to a large group of anionic clays. Their layered structure consists of brucite-like layers with octahedrally centred Mg^{2+} ions and some isomorphously substituted Al^{3+} ions creating positive charge that is compensated with different anions present in the interlayer region together with water [7–9]. The general

formula for these materials is: $[M(II)_{1-x}\ M(III)_x(OH)_2](A^{n-})_{x/n}\cdot m\ H_2O$, where M(II) is a divalent cation, such as Mg^{2+}, Fe^{2+}, Co^{2+}, Cu^{2+}, Ni^{2+}, Zn^{2+} or Ca^{2+}; M(III) is a trivalent cation, such as Al^{3+}, Fe^{3+}, Cr^{3+}, Mn^{3+}, Co^{3+} or La^{3+}; A^{n-} is anion (usually carbonate) and $x = M(III)/[(M(II) + M(III)]$. Their acid–base and redox properties can be tailored by the variation of M(II)/M(III) ratio or by isomorphous substitution with different M(II) and M(III) ions. Owing to limited thermal stability LDHs can easily form mixed oxide phases upon thermal treatment, with homogeneous interdispersion of constituting elements and desirable properties, such as large surface area and improved resistance against sintering compared to supported catalysts [1, 2, 9, 10]. The maximum extent of the M(III) substitution into LDH framework is expected to be at $x \sim 0.3$ [1, 9, 11, 12], but higher aluminium substitution ($x \sim 0.45$) has also been reported [13]. The substitution of M(III) ions provides an intimate contact between two or more oxide components influencing the properties potentially favourable in catalytic processes.

The aim of this study was to investigate the influence of the synthesis method and of constituent metal (Mg, Al and Fe) content on the thermal stability of Mg–Al LDH and Mg–Al–Fe LDHs. The conversion of LDHs to mixed oxides by thermal decomposition and the transition stages temperatures were used as the indication of thermal stability of LDHs.

Two different coprecipitation methods, low supersaturation (LS) and high supersaturation (HS), were chosen for the synthesis of LDHs. In this study, the content of trivalent ions was varied in a wide range between $0.15 < x < 0.7$ exceeding the optimal range for the single LDH phase synthesis ($0.20 < x < 0.33$) [1]. The intention was to induce the formation of different LDHs and consequently obtain, after thermal treatment, different multiphase mixed oxides.

Experimental

Synthesis of LDHs

Various preparation methods are described in the literature [6, 9, 14–16], but the most commonly used for the LDH synthesis are coprecipitation methods. Two different coprecipitation methods were chosen for the synthesis of LDHs: high supersaturation (denoted as HS) and low supersaturation with constant pH (denoted as LS) [17, 18].

Before each coprecipitation, 1 dm^3 of 1 M solution (regarding to metal content) with the wanted Mg:Al:Fe ratio was prepared. Magnesium, aluminium and iron nitrate salts were used. The anionic constituents, CO_3^{2-} and OH^- ions, necessary for the LDH formation were obtained from 1 dm^3 solution containing Na_2CO_3 and NaOH with the following concentrations: $CO_3^{2-}/(M(III) + Mg) = 0.67$ and $OH^-/(M(III) + Mg) = 2.25$.

In the HS method, the solution of metal precursors was quickly added to the second solution containing Na_2CO_3 and NaOH. For the LS synthesis, the solution containing the M(II) and M(III) ions was added at a constant rate (4 $cm^3\ min^{-1}$) into 1 dm^3 of distilled water and the pH of the solution was maintained between 9.6 and 9.9 by the simultaneous addition of the second solution containing Na_2CO_3 and NaOH.

In both cases, the reaction solution was vigorously stirred at temperature of 40 °C, after which the samples were aged for 15 h under the same conditions and then washed and filtered several times with warm distilled water (40 °C) until the pH of the washing water reached 7.0. The precipitates were dried for 24 h, at 100 °C in air, and afterwards calcined for 5 h, at 500 °C in air.

For the samples denotation the synthesis method (HS or LS) and the initial molar metal ratio was chosen (e.g. HS-Mg70Al25Fe5 is the denotation for the sample synthesized by the HS method having following initial metal amounts: 70 mol% of magnesium, 25 mol% of aluminium and 5 mol% of iron).

Characterization

XRD measurements were performed in a Siemens D500 X-ray diffractometer (Cu K_α radiation, $\lambda = 0.154$ nm, 45 kV, 25 mA) in 2θ range from 3° to 63°.

The elemental chemical analysis of constituent metals (Mg, Al and Fe) was performed by atomic adsorption spectroscopy, AAS using Hitachi Z-6100 instrument, whereas micro elemental chemical analysis was achieved by multipoint investigation of sample surface using JEOL, JSM-460 LV instrument equipped with energy dispersive spectroscopy, EDS, Oxford Instruments INCA X-sight system operating at 25 kV.

For the thermal analysis (TG, DTA) Baehr STA503 instrument was used. All synthesized samples were analyzed from ambient temperature to 1,000 °C with the heating rate of 5 °C min^{-1}.

Results and discussion

All coprecipitation products have XRD patterns typical for LDH compounds (Fig. 1) [9, 19]. Sharp and symmetric reflections from (003), (006), (110) and (113) planes were observed as well as broad, non-symmetric reflections from (102), (105) and (108) planes. The structure parameters from all samples, obtained from XRD measurements, are listed in Table 1. The lattice parameters were calculated for

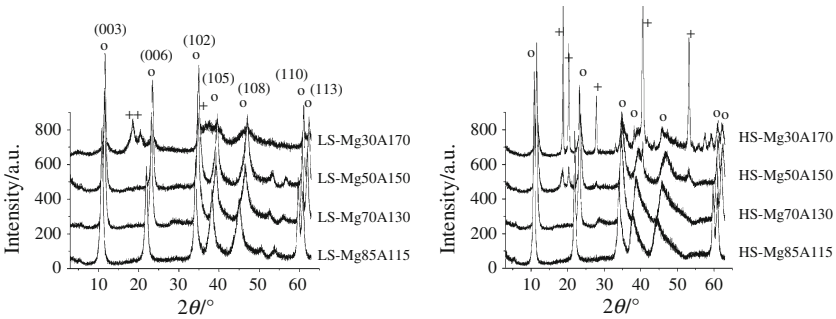

Fig. 1 XRD patterns of synthesized Mg–Al samples (*o* LDH; + Bayerite)

Table 1 Precipitation products phase composition and lattice parameters

Sample	XRD phase	d_0/nm	a_0/nm	c_0/nm	Sample	XRD phase	d_0/nm	a_0/nm	c_0/nm
HS-Mg85Al15	LDH	0.813	0.309	2.440	HS-Mg85Al10-Fe5	LDH	0.805	0.310	2.416
HS-Mg70Al30	LDH	0.766	0.305	2.299	HS-Mg70Al25-Fe5	LDH	0.762	0.306	2.287
HS-Mg50Al50	LDH + Bayerite	0.760	0.303	2.279	HS-Mg50Al45-Fe5	LDH + Bayerite	0.759	0.303	2.278
HS-Mg30Al70	LDH + Bayerite	0.764	0.304	2.291	HS-Mg30Al65-Fe5	LDH + Bayerite	0.758	0.302	2.274
LS-Mg85Al15	LDH	0.813	0.309	2.440	LS-Mg85Al10-Fe5	LDH	0.793	0.310	2.381
LS-Mg70Al30	LDH	0.766	0.305	2.299	LS-Mg70Al25-Fe5	LDH	0.763	0.306	2.289
LS-Mg50Al50	LDH	0.759	0.303	2.277	LS-Mg50Al45-Fe5	LDH	0.755	0.302	2.266
LS-Mg30Al70	LDH + Bayerite	0.754	0.303	2.261	LS-Mg30Al65-Fe5	LDH + Bayerite	0.764	0.301	2.293

a hexagonal unit cell on the basis of rhombohedral R—3m symmetry [19–21]. Basal spacing $d_0 = d_{003}$ was calculated as the thickness of one layer constituted of one brucite-like sheet and one interlayer, cation–cation distance within the brucite-like layer as $a_0 = 2{\cdot}d_{110}$ and lattice parameter c_0 as $c_0 = 3{\cdot}d_{003}$.

It was observed that with the increase of M(III) content, the intensity of characteristic XRD reflections decreases. HS samples have more intense XRD reflections at 2θ values smaller than 30° and lower symmetry of peaks at higher 2θ values. This asymmetry of reflections for HS samples is due to the partially disordered structure, particularly, turbostratic random arrangement of the layers which are not neatly stacked but have random arrangement [22]. In addition to the detected LDH phase in all samples with $x = 0.7$ and HS samples with $x = 0.5$ the presence of aluminium hydroxide, $Al(OH)_3$—bayerite was observed, the reflections being more intense for HS samples. The LS synthesis method allows the formation of LDHs with an extended M(III) substitution ($x = 0.5$), evidenced by the shortened lattice parameter a_o of the hexagonal lattice (Table 1). Lattice parameter a_o is in strong correlation with the amount of M(III) incorporated into LDHs matrix [9, 11, 13, 23] and decreases with the increase in M(III) amount.

With the increase in M(III) amount a decrease in basal spacing is observed due to the stronger attraction between negatively charged hydroxide layers and interlayer anions. The exception are the HS-Mg30Al70 and LS-Mg30Al65Fe5 samples probably because these samples also have an additional bayerite phase suggesting that the amount of aluminium incorporated into the LDH matrix is smaller than for the corresponding samples with $x = 0.5$.

The presence of 5 mol% of iron decreases and broadens the diffraction lines (Fig. 2), but has the same trend as in series of samples without iron. Also a decreases the basal spacing for Mg–Al–Fe samples (exception being the LS

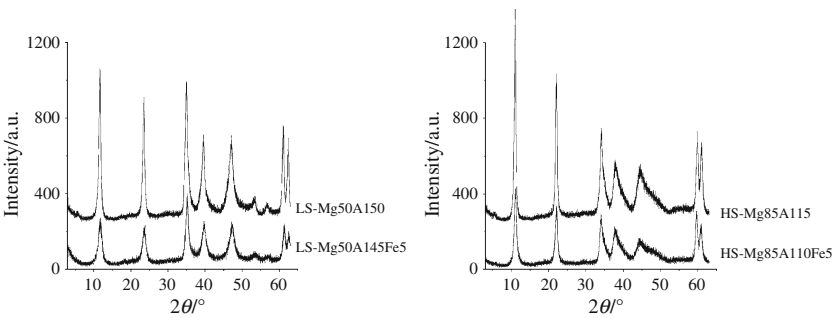

Fig. 2 XRD patterns of the Mg–Al and Mg–Al–Fe samples synthesized with the same amount of M(III)

samples with $x = 0.7$) was observed when compared to Mg–Al samples.

After thermal treatment at 500 °C layered structure was destroyed, since the XRD patterns of calcined samples showed only broad reflections of Mg/M(III) mixed oxides. These mixed oxides have regular network from cubic close packed oxygen ions with M(III) ions in interstitial space [23]. For all calcined samples, XRD measurements did not detect any formation of pure M(III)-oxides after calcination at 500 °C.

Visually observed, the Mg–Al samples are have white, whereas the addition of iron gives orange-brownish colouring of Mg–Al–Fe samples. For the samples with 5% iron, the increase in Al content intensifies the colouring of samples (Table 2). The colour of iron containing HS samples is darker than the colour of LS samples. The Mg–Al–Fe samples with iron incorporated in LDH framework should be white, since the isolated Fe^{3+} ions in octahedral coordination sites in LDHs do not give rise to any coloration, as reported in literature [24]. The coloration of Fe containing LDHs suggests the presence of extra framework iron and can be associated with the presence of bulk iron oxide phases. It must be noted that the XRD analysis did not detect any reflections belonging to $Fe(OH)_3$ but nevertheless this does not exclude the presence of some amorphous phases.

For detailed elemental chemical analysis of constituent metals two different methods were selected: AAS analysis for the bulk and EDS analysis for the surface-enhanced information about metal composition. AAS analysis showed higher presence of magnesium, and consequently, lower presence of aluminium in the material bulk when compared to the initial amount for all synthesized samples (Table 3). This suggests that a portion of aluminium was not incorporated into the LDH matrix (or bayerite in multiphase samples) and that it must have been washed out during the washing and filtering period of sample preparation. The small amount of iron in Mg–Al–Fe samples was similar to the initial amount. When comparing different synthesis methods, the most pronounced difference between samples having the same initial composition was observed for the multiphase Mg–Al samples, whereas the composition of other samples detected by AAS was almost the same. These differences could be explained by the larger amount of Bayerite phase present in HS samples confirmed by more intense XRD reflections.

Table 2 The colour of the precipitation products

Sample	Precipitate colour	Sample	Precipitate colour
HS-Mg85Al10-Fe5	White	LS-Mg85Al10-Fe5	White
HS-Mg70Al25-Fe5	Beige	LS-Mg70Al25-Fe5	Beige
HS-Mg50Al45-Fe5	Dark orange-brown	LS-Mg50Al45-Fe5	Pale orange
HS-Mg30Al65-Fe5	Dark orange-brown	LS-Mg30Al65-Fe5	Pale orange

Table 3 The initial metal amounts and the metal amounts measured by AAS and EDS

Sample	Initial amounts/mol%			Amounts measured by AAS/mol%			Amounts measured by EDS/mol%		
	Mg	Al	Fe	Mg	Al	Fe	Mg	Al	Fe
HS-Mg85Al15	85	15	–	87.1	12.9	–	85.9	14.1	–
HS-Mg70Al30	70	30	–	75.7	24.3	–	71.9	28.1	–
HS-Mg50Al50	50	50	–	57.2	42.8	–	58.0	42.0	–
HS-Mg30Al70	30	70	–	40.0	60.0	–	32.4	67.6	–
HS-Mg85Al10-Fe5	85	10	5	86.9	8.4	4.7	82.9	7.8	9.2
HS-Mg70Al25-Fe5	70	25	5	73.6	21.6	4.8	72.9	18.7	8.4
HS-Mg50Al45-Fe5	50	45	5	55.0	40.1	4.9	49.6	42.2	8.2
HS-Mg30Al65-Fe5	30	65	5	33.8	60.9	5.3	30.3	65.9	3.8
LS-Mg85Al15	85	15	–	87.2	12.8	–	87.0	13.0	–
LS-Mg70Al30	70	30	–	74.0	26.0	–	76.5	23.5	–
LS-Mg50Al50	50	50	–	65.9	34.1	–	63.0	37.0	–
LS-Mg30Al70	30	70	–	35.2	64.8	–	32.7	67.3	–
LS-Mg85Al10-Fe5	85	10	5	87.0	8.5	4.5	86.9	8.0	5.2
LS-Mg70Al25-Fe5	70	25	5	73.5	21.7	4.8	75.0	21.2	3.8
LS-Mg50Al45-Fe5	50	45	5	54.9	40.0	5.1	57.6	39.9	2.5
LS-Mg30Al65-Fe5	30	65	5	33.4	61.4	5.2	34.3	62.9	2.8

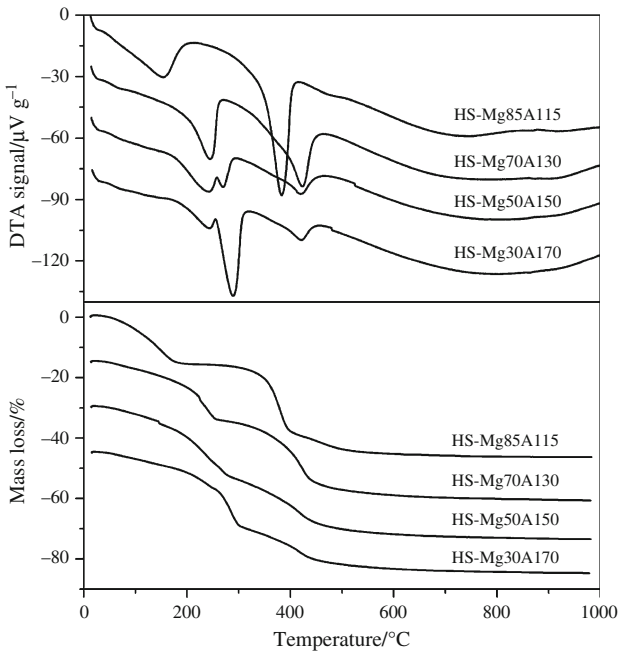

Fig. 3 TG and DTA curves from HS-Mg–Al samples

The EDS analysis revealed similar magnesium amount on the surface as in the bulk of material (Table 3). However, the iron amount on the surface differs from the bulk amount being higher than the initial amount in HS-Mg–Al–Fe samples (exception: HS-Mg30Al65Fe5 sample having lower amount). For the LS-Mg–Al–Fe samples the amount of iron on the surface is smaller (exception: LS-Mg85Al10Fe5 sample having similar amount) than the initial amount, and consequently, the aluminium amount differs from the bulk amount. These observations could be explained by the larger structure distortion especially in stacking of layers which expelled some of iron ions onto the surface of HS-Mg–Al–Fe samples. Furthermore, this explanation is supported by the more intense colouration of these samples originating form iron ions not incorporated into the LDH framework. On the contrary, the iron amount in LS-Mg–Al–Fe samples is smaller probably due to the washing out of iron ions during the sample preparation.

The thermal behaviour of the coprecipitation products was investigated with TG–DTA analysis. All samples have two endothermic transitions with corresponding mass losses (Fig. 3) typical for the LDHs [24–30].

The first transition comes from the loss of physisorbed and interlayer water, without the collapse of layered structure. At this point, M(III) ions migrate into interlayer and switch from octahedral to tetrahedral coordination [31]. In the case of excess M(III) content ($x > 0.5$), two endothermic peaks are observed during the first transition because of the presence of an additional bayerite phase and its dehydroxylation before the second transition.

The second mass loss, due to the loss of hydroxyl groups from brucite-like layer and the loss of interlayer anions, is almost the same for all samples with the same M(III) amount, the exception being the single LDH phase LS-Mg50Al50 and LS-Mg50Al45Fe5 samples compared to the multiphase HS-Mg50Al50 and HS-Mg50Al45Fe5 samples. A decrease in second mass loss (Fig. 3) was observed with an increase in M(III) ion amount. The explanation is the partial loss of OH^- from brucite-like layers before the second main transition reported also in literature [9], and for the bayerite containing samples, smaller amount of compensating anions in LDH interlayer.

Both main endothermic transitions could emerge as doubled endothermic effects (Table 2; Figs. 3, 5) depending quantitatively and qualitatively from many different factors such as: M(II)/M(III) ratio, anion type, low temperature treatment (drying after coprecipitation) and thermal treatment atmosphere [9, 29]. After the second transition, a very mild mass loss continues probably due to the loss of leftover interlayer anions. Another endothermic transition without significant mass loss is observed between 680 and 830 °C indicating stoichiometric spinel phase and single magnesium-oxide phase formation.

Figure 4 shows mass losses vs. M(III) ion ratio x and the data from the DTA analysis is listed in Table 4. A general observation can be made that the Mg–Al-LDH samples obtained by both, HS and LS method have larger total mass loss when compared to the Mg–Al–Fe-LDH samples. With the increase in M(III) amount in samples the total mass loss and the second mass loss decrease, whereas the first mass loss increases.

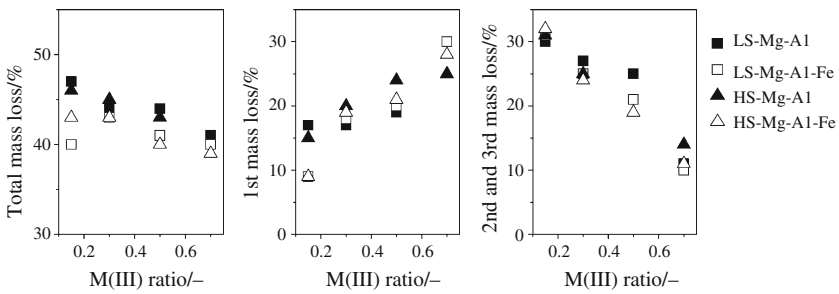

Fig. 4 Total mass loss (*left*), mass loss of the first transition stage (*middle*) and second plus third transition stage (*right*) vs. M(III) ion ratio x of all synthesized samples

Table 4 Data from DTA analysis: the temperatures of endothermic peaks corresponding to the first transition T_1 and T_1', to the second transition T_2 and to the third transition T_3

Sample	T_1 and T_1'/°C	T_2 and T_2'/°C	T_3/°C	Sample	T_1 and T_1'/°C	T_2 and T_2'/°C	T_3/°C
HS-Mg85Al15	156	381, 479	735	LS-Mg85Al15	141	384, 468	730
HS-Mg70Al30	244	423	786	LS-Mg70Al30	213	348, 409	684
HS-Mg50Al50	243, 270	421	801	LS-Mg50Al50	207, 228	411	688
HS-Mg30Al70	243, 289	421	811	LS-Mg30Al70	218, 257	406	722
HS-Mg85Al10-Fe5	149	376, 469	679	LS-Mg85Al10-Fe5	144	379, 453	684
HS-Mg70Al25-Fe5	236	418	827	LS-Mg70Al25-Fe5	213	356, 405	691
HS-Mg50Al45-Fe5	243, 274	420	819	LS-Mg50Al45-Fe5	121, 197	410	683
HS-Mg30Al65-Fe5	245, 270	417	735	LS-Mg30Al65-Fe5	210, 256	406	684

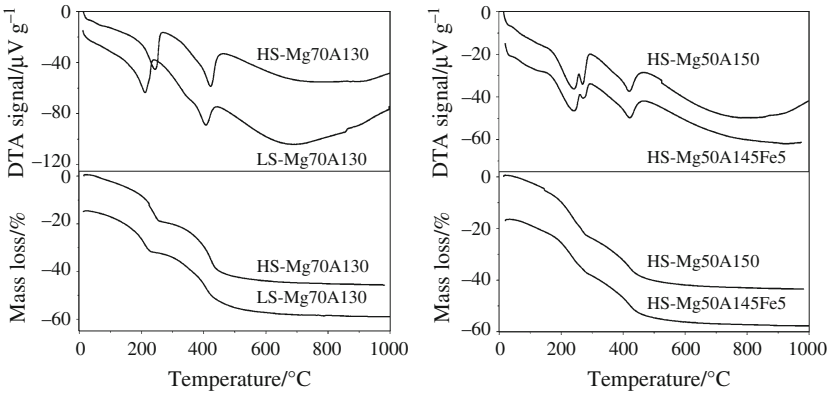

Fig. 5 The influence of the synthesis method (*left*) and of the presence of small amount of iron as ternary metal (*right*) on thermal decomposition od LDHs

The mass losses of both transition stages for the Mg–Al–Fe-LDH samples, obtained by HS and LS method, as well as the temperatures of the characteristic DTA peaks, do not differ significantly when compared to the Mg–Al-LDH samples with the same M(III) amount. The exception being the Mg–Al–Fe-LDH samples with $x = 0.15$ which have lower total mass loss than the Mg–Al-LDH samples due to the lower total mass loss resulting from lower content of interlayer water released in the first transition. This water content may be related to the strength of hydrogen bonding with the hydroxyl layer and to the degree of order within the layer. The XRD analysis showed that the iron containing materials have lower crystallinity, which could be the indication of lower structural order. Such an effect is of particular importance for the Mg–Al–Fe-LDH samples with $x = 0.15$, which have the largest influence of iron ions since they constitute 1/3 of the total M(III) content.

The temperatures of the second and third thermal transition increase and their intensities decrease with the increase in M(III) ion amount in samples. It was observed that the DTA peak shifts toward higher temperatures with the increase in M(III) ion amount. This shift could be explained by the increase in charge density of hydroxyl layers and by the larger number of hydrogen bonds [32].

All samples prepared by the HS method have higher temperature of both transitions compared to LS samples with the same composition indicating that a more stable layered structure can be obtained with HS method (Table 4; Fig. 5). The comparison of samples with same amount of M(III) ions reveals that iron containing samples have lower temperatures of both transitions than those without iron (Table 4; Fig. 5), and thus also have less stable layered structure referring that the presence of aluminium in LDHs stabilizes layered structure.

Conclusions

The synthesis method influences structural, physicochemical and thermal properties of created LDHs. Compared to HS synthesis method, the LS method allows the formation of LDHs with an extended M(III) substitution ($x = 0.5$). XRD analysis also showed partially disordered structure in stacking of layers for all HS samples, which was not observed for LS samples. The EDS chemical analysis revealed, for the HS iron containing samples, larger iron amount on the surface than in the bulk. These finding could be explained with the larger distortion in structure compared to LS samples which expelled some of iron ions onto the surface in HS-Mg–Al–Fe samples, as well as with the visually observed more intense coloration of HS samples originating from extra framework iron ions.

The LS samples of the same initial composition showed lower thermal stability compared to the HS samples estimated by lower temperature of both thermal decomposition stages (first stage being the loss of physisorbed and interlayer water, and the second dehydroxylation of hydroxyl groups and decarboxylation of anions from interlayer). The thermal stability of LDHs was not influenced considerably with the introduction of a small amount of iron as ternary metal even though lower crystallinity of Mg–Al–Fe LDHs was observed.

Acknowledgements The financial support received from DAAD, 38th International Seminar for Research and Teaching in Chemical Engineering and Physical Chemistry, Universität Karlsruhe, Germany and from Serbian Ministry of Education and Science (Contract No. II145008) is gratefully acknowledged.

References

1. Vaccari A. Preparation and catalytic properties of cationic and anionic clays. Catal Today. 1998;41:53–71.
2. Serwicka EM, Bahranowski K. Environmental catalysis by tailored materials derived from layered minerals. Catal Today. 2004;90:85–92.
3. Ambrogi V, Perioli L, Ricci M, Pulcini L, Nocchetti M, Giovagnoli S, Rossi C. Eudragit® and hydrotalcite-like anionic clay composite system for diclofenac colonic delivery. Microporous Mesoporous Mater. 2008;115:405–15.
4. El Gaini L, Lakraimi M, Sebbar E, Meghea A, Bakasse M. Removal of indigo carmine dye from water to Mg–Al–CO_3-calcined layered double hydroxides. J Hazard Mater. 2009;161:627–32.
5. Xu ZP, Zhang J, Adebajo MO, Zhang H, Zhou C. Catalytic applications of layered double hydroxides and derivatives. Appl Clay Sci. 2011;53:139–50.
6. Goh KH, Lim TT, Dong Z. Application of layered double hydroxides for removal of oxyanions: a review. Water Res. 2008;42:1343–68.
7. Reichle WT. Synthesis of anionic clay minerals (mixed metal hydroxides, hydrotalcite). Solid States Ionics. 1986;22:135–41.
8. Newman SP, Jones W. Supramolecular Organisation and Material Design. In: Jones W, Rao CNR, editors. Cambridge University Press. Cambridge: UK; 2002. p. 295–331.
9. Cavani F, Trifitro F, Vaccari A. Hydrotalcite-type anionic clays: preparation, properties and applications. Catal Today. 1991;11:173–301.
10. Carrado KA, Kostapapas A. Layered double hydroxides (LDHs). Solid State Ionics. 1988;26:77–86.
11. Miyata S. Physico-chemical properties of synthetic hydrotalcites in relation to composition. Clays Clay Min. 1980;28:50–6.
12. Evans D, Slade RCT. Structural aspects of layered double hydroxides. Struct Bond. 2006;119:1–87.
13. Tsuji M, Mao G, Yoshida T, Tamaura Y. Hydrotalcites with extended Al^{3+}-substitution: synthesis, simultaneous TG-DTA-MS study, and their CO_2 adsorption behaviors. J Mater Res. 1993;8(5):1137–42.
14. Olsbye U, Akporiaye D, Rytter E, Ronnekleiv M, Tangsatd E. On the stability of mixed M^{2+}/M^{3+} oxides. Appl Catal A Gen. 2002;224:39–49.
15. Prineto F, Ghiotti G, Durand R, Tichit D. Investigation of acid-base properties of catalysts obtained from layered double hydroxides. J Phys Chem B. 2000;104:11117–26.
16. Adachi-Pagano M, Forano C, Besse JP. Synthesis of Al-rich hydrotalcite-like compounds by using the urea hydrolysis reaction—control of size and morphology. J Mater Chem. 2003;13:1988–93.
17. Chen YZ, Hwang CM, Liaw CW. One-step synthesis of methyl isobutyl ketone from acetone with calcined Mg/Al hydrotalcite-supported palladium or nickel catalysts. Appl Catal A Gen. 1998;169:207–14.
18. Hadnadjev M, Vulic T, Marinkovic-Neducin R, Suchorski Y, Weiss H. The iron oxidation state in Mg–Al–Fe mixed oxides derived from layered double hydroxides: an XPS study. Appl Surf Sci. 2008;254:4297–302.
19. Miyata S. The synthesis of hydrotalcite-like compounds and their structures and physico-chemical properties-I. The systems Mg^{2+}–$A1^{3+}$–NO_3^-, Mg^{2+}–$A1^{3+}$–$C1^-$, Mg^{2+}–$A1^{3+}$–ClO_4^-, Ni^{2+}–$A1^{3+}$–$C1^-$, and Zn^{2+}–Al^{3+}–Cl^-. Clays Clay Min. 1975;25:369–75.
20. Carja G, Nakamura R, Niiyama H. Copper and iron substituted hydrotalcites: properties and catalyst precursors for methylamines synthesis. Appl Catal A Gen. 2002;236:91–102.
21. Meloni D, Sini MF, Cutrufello MG, Monaci R, Rombi E, Ferino I. Characterization of the active sites in MgNiAl mixed oxides by microcalorimetry and test reaction. J Therm Anal Calorim. 2011. doi:10.1007/s10973-011-2031-6.
22. Stanimirova T, Balek V. Characterization of layered double hydroxide Mg–Al–CO_3 prepared by re-hydration of Mg–Al mixed oxide. J Therm Anal Cal. 2008;94(2):477–81.
23. Kaneyoshi M, Jones W. Formation of Mg–Al layered double hydroxides intercalated with nitrilotriacetate anions. J Mater Chem. 1999;9:805–11.
24. Ohishi Y, Kawabata T, Shishido T, Takaki K, Zhang Q, Wang Y, Nomura K, Takehira K. Mg–Fe–Al mixed oxides with mesoporous properties prepared from hydrotalcite as precursors: catalytic behavior in ethylbenzene dehydrogenation. Appl Catal A Gen. 2005;288:220–31.
25. Stanimirova T, Hibino T, Balek V. Thermal behavior of Mg–Al–CO_3 layered double hydroxide characterized by emanation thermal analysis. J Therm Anal Cal. 2006;84(2):473–8.
26. Spratt HJ, Palmer SJ, Frost RL. Thermal decomposition of synthesised layered double hydroxides based upon Mg/(Fe, Cr) and carbonate. Thermochim Acta. 2008;47:1–6.
27. Wu Y, Bai H, Zhou J, Chen C, Xu X, Xu Y, Qian G. Thermal and chemical stability of Cu–Zn–Cr-LDHs prepared by accelerated carbonation. Appl Clay Sci. 2009;42:591–6.
28. Kovanda F, Rojka T, Bezdicka P, Jiratova K, Obalova L, Pacultova K, Bastl Z, Grygar T. Effect of hydrothermal treatment on properties of Ni–Al layered double hydroxides and related mixed oxides. J Solid State Chem. 2009;182:27–36.
29. Wegrzyn A, Rafalska-Łasocha A, Majda D, Dziembaj R, Papp H. The influence of mixed anionic composition of Mg–Al hydrotalcites on the thermal decomposition mechanism based on in situ study. J Therm Anal Calorim. 2010;99:443–57.
30. Chmielarz L, Rutkowska M, Kustrowski P, Drozdek M, Piwowarska Z, Dudek B, Dziembaj R, Michalik M. An influence of thermal treatment conditions of hydrotalcite-like materials on their catalytic activity in the process of N_2O decomposition. J Therm Anal Calorim. 2011;105:161–70.
31. Belloto M, Rebours B, Clause O, Lynch J, Bazin D, Elkaim E. Hydrotalcite decomposition mechanism: a clue to the structure and reactivity of spinel-like mixed oxides. J Phys Chem. 1996;100:8535–42.
32. Yun SK, Pinnavaia TJ. Water content and particle texture of synthetic hydrotalcite-like layered double hydroxides. Chem Mater. 1995;7:348–54.